ORIGINAL PAPER

Rheology, Morphology and Thermal Properties of a PLA/PHB/Clay Blend Nanocomposite: The Influence of Process Parameters

Alessandra D'Anna[1] · Rossella Arrigo[1] · Alberto Frache[1]

Abstract

The effect of process parameters on the final properties of a poly-lactic acid (PLA) and polyhydroxybutyrate (PHB) polymer blend filled with nanoclays was evaluated. To this aim, the nanofilled blend was processed in a co-rotating twin screw extruder, considering three different screw profiles and different values of the screw rotation speed, and the thermal and thermo-mechanical properties of the so-obtained materials were investigated. Furthermore, XRD analyses, SEM observations and rheological characterization were exploited to infer the coupled effect of the process parameters and nanoclay presence on the microstructure of the filled blend. Preliminary thermodynamic calculations allowed predicting the preferential localization of the nanoclay in the interfacial region between the polymeric phases. The relaxation mechanism of the particles of the dispersed phase in nanofilled blend processed, by rheological measurements, is not fully completed due to an interaction between polymer ad filler in the interfacial region with a consequent modification of the blend morphology and, specifically, a development of an enhanced microstructure. Therefore, by varying the screw configuration, particularly the presence of backflow and distribution elements in the screw profile, high shear stresses are induced during the processing able to allow a better interaction between polymers and clay. This finding also occurs in the thermo-mechanical properties of material, as an improvement of storage modulus up to 20% in filled blend processed with a specific screw profile. Otherwise, the microstructure of filled blend processed with different screw speed is similar, according to the other characterizations where no remarkable alterations of materials were detected.

Keywords Bio-based polymer blend · Nanocomposite · Screw profile · Screw speed · Rheological behavior · Morphology

Introduction

Bio-based plastics have attracted increased interest as a potential solution to the problems created by the intensive use of petroleum-derived plastics [1]. Bio-based polymers, obtained from natural resources, include polylactic acid PLA [2, 3], polyhydroxybutyrate PHB [4, 5], thermoplastic starch [6, 7], cellulose and its derivatives [8]. These materials are broadly studied due to their fundamental characteristics [9]: values of tensile strength and elastic modulus which are similar to those of polymers of synthetic origin [10]. Nevertheless, several characteristics, as brittleness and poor barrier properties, restrict their range of application [11]. To overcome these limits, different strategies have been proposed; one of the most successful methods is blending with other bio-polymers. Blending is a much more practical and cost-effective method with respect to other strategies and, for this purpose, it is a frequently used method in the industrial sector [12]. Some studies are present in literature documenting the melt blending with biodegradable or synthetic polymers [13–17].

In this regard, PLA/PHB blends have been widely studied [18–20]. However, PLA-PHB polymer blends are immiscible and therefore, to obtain a material with enhanced final properties, a modification of the blend is often necessary. This problem can be solved by using appropriate compatibilizers, as in our previous study [21], by using chemically modifying polymers, or by mixing polymers with nanofillers

✉ Alberto Frache
   alberto.frache@polito.it

   Alessandra D'Anna
   alessandra.danna@polito.it

   Rossella Arrigo
   rossella.arrigo@polito.it

[1] Department of Applied Science and Technology, Polytechnic of Turin, INSTM Local Unit, Viale Teresa Michel 5, 15121 Alessandria, Italy

during the processing in order to induce a better molecular interaction between the two polymeric phases involved in the blend. In particular, the use of nanofillers, is very important due to the capability of these particles to enhance the properties of the material even at low contents, namely, below 10 wt% [22]. A huge variety of nanoparticles have been used in the production of nanocomposites [23, 24], among these the nanoclays. The microstructures and properties of the nanocomposites depend on many factors: the interaction between the polymers and the nanoclays, the type and the content of the nanoclays and the localization of the used filler. Sivanjineyulu et al. investigated the selective localization of carbon nanotubes (CNTs) and organoclays in biodegradable poly(butylene succinate) (PBS)/PLA blend-based nanocomposites. In the hybrid composites, the CNTs were preferentially located in the continuous PBS matrix, while the organoclay settled in the PLA phase. The preferential localization of the organoclays in the PLA domains was ascribed to the interactions between PLA and the organically modified surface of clay [25]. Besides, Zembouai et al. studied a PHBV/PLA blend with sepiolite and cloisite C30B. Although a good degree of dispersion of fillers in the blends and the absence of aggregates were achieved, but the preferential location of the fillers was not discussed [26].

In addition to the blend composition, the morphology of polymer blends is affected by processing parameters. In particular, since twin-screw extruders have most widely been used to prepare polymer blends at industrial level, in the last years numerous research groups have investigated the effect of process parameters on the morphology evolution of polymer blends [27]. As an example, Decol et al. studied the influence of both the presence of filler and the variation of process parameters in a blend Poly(ε-Caprolactone) PCL/PLA [28]. Hejazi et al. studied the influence of process parameters on mechanical properties of Polypropylene/Ethylene–Propylene–Diene–Monomer/clay nanocomposites concluding that the high toughness of material requires moderate levels of organoclay (from 3 to 5 wt%) and screw speed at 240 rpm. Therefore, processing parameters are an essential factor for the final properties of a nanocomposite material [29].

The aim of this work was to evaluate the influence of the process parameters, such as screw profile and screw rotation speed on the morphology and properties of a PLA/PHB/clay blend nanocomposite. Although several papers dealing with the formulation and characterization of biopolymer-based filled blends are reported in the scientific literature, the role of the processing parameters, especially as far as the influence of the screw profile is concerned, in modifying the microstructure and the final properties of these materials has not been systematically elucidated yet. In fact, for the full exploitation of biopolymer blends also at industrial scale, the evaluation of their processing behavior and the optimization of the processing conditions is of fundamental importance. Therefore, in this study, a twin-screw extruder was used to process the blend nanocomposites, and the morphology and the thermal and mechanical properties of the resulting materials, as well as the clay localization were evaluated. Additionally, a detailed study of the rheological response of the blend nanocomposites was performed, aiming at correlating the process parameters with the obtained material microstructure.

Materials and Methods

Materials

PLA was supplied in pellets form by IngeoTM Natural Natureworks under the trade name PLA3251D. The polymer main properties are: density = 1.24 g/cm^3, MFI = 33 g/10 min (210 °C, 2.16 kg).

PHB was manufactured by Aonilex, KANEKA Biopolymer under the trade name PHBX151A. The used PHB has the following characteristics: density = 1.19 g/cm^3, MFI = 3 g/10 min (165 °C, 5 kg). The polymers were commercialized in pellets form.

Cloisite 5 bentonite organo-modified with bis(hydrogenated tallow alkyl)dimethyl salt was supplied by BYK Additives & Instruments, ALTANA in powder form. The used filler has a density of 1.77 g/cm^3.

Preparation of the Blends

The polymers were first dried for 5 h at 80 °C in a vacuum oven and then the neat PLA/PHB 70/30 wt% blend and the filled systems, whose formulations are reported in Table 1, were prepared using a co-rotating twin screw extruder LEISTRITZ ZSE 18/40D with the following characteristics: diameter Φ = 18 mm and L/D ratio = 40. The extrusion flow rate has been maintained at 3 kg/h. The barrel temperature was set from 170 to 190 °C, as shown in Fig. 1a, along the extruder axis and the melt temperature was measured to be 185 °C. Two gravimetric feeders were used: a principal feed for the polymers (PLA 70 wt%, PHB 30 wt%), which was positioned at the beginning of the screw and a second side feeder for the clay. The filled blends were processed using three different screw profiles (Fig. 1) at 400 rpm. In addition, maintaining fixed screw profile 3, the screw speed was changed (250, 400 and 550 rpm). A preliminary study was performed on unfilled blends and, since their morphology was almost unaffected by the different screw profiles, only the results regarding screw profile 1 were reported in the paper. At the end of each extrusion run, the material leaving the extruder was passed into a cooling tank and pelletized. Specimens for the different characterizations were prepared

Table 1 Composition and code of the studied polymer blend (all percentages are referred as wt%)

Composition	Code
PLA: 70 wt% and PHB: 30 wt%	PLA/PHB
Polymer blend 95 wt% and Cloisite 5: 5 wt%; Screw 1; 400 rpm	PLA/PHB/CL/1/400
Polymer blend 95 wt% and Cloisite 5: 5 wt%; Screw 2; 400 rpm	PLA/PHB/CL/2/400
Polymer blend 95 wt% and Cloisite 5: 5 wt%; Screw 3; 400 rpm	PLA/PHB/CL/3/400
Polymer blend 95 wt% and Cloisite 5: 5 wt%; Screw 3; 250 rpm	PLA/PHB/CL/3/250
Polymer blend 95 wt% and Cloisite 5: 5 wt%; Screw 3; 550 rpm	PLA/PHB/CL/3/550

Fig. 1 **a** Temperature profile **b** Screw profile 1 **c** Screw profile 2 **d** Screw profile 3
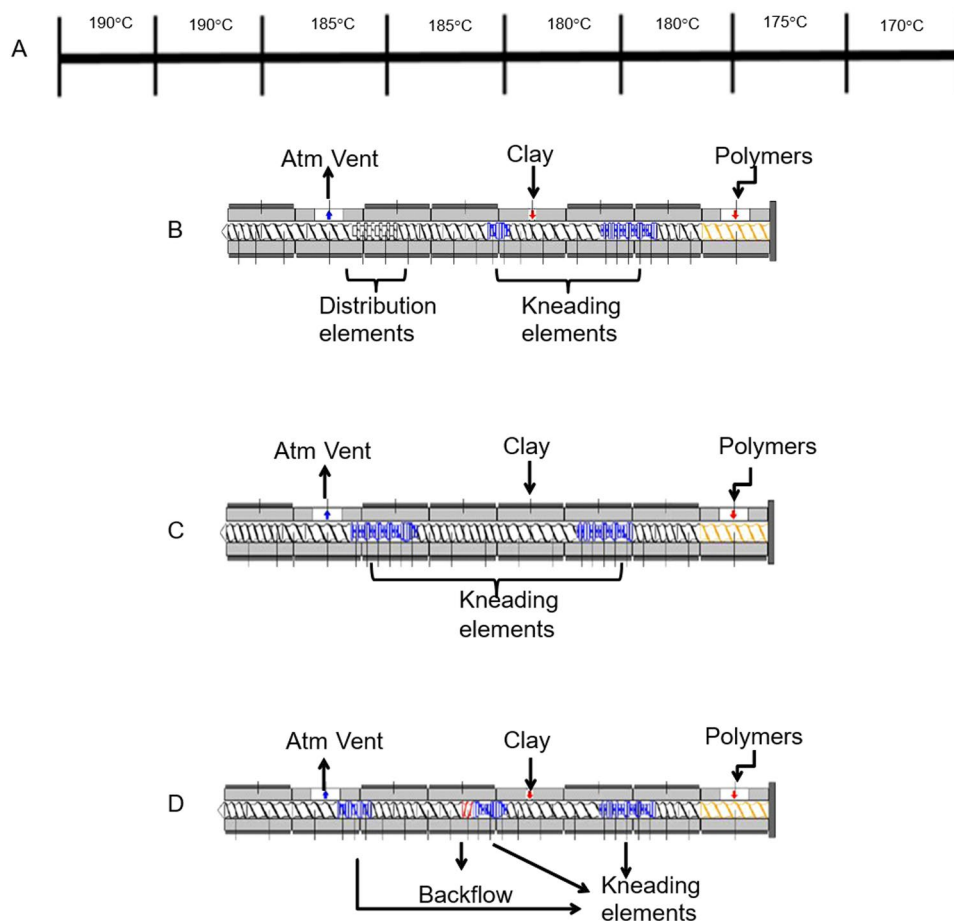
through a compression molding step in a laboratory press (Collin Teach Line 200 T) working at 100 bar and 190 °C for 3 min.

Characterizations

Differential Scanning Calorimetry (DSC)

DSC measurements were carried on weighted samples of about 8 mg placed in sealed aluminum pans using a Q20 TA Instrument (New Castle, DE, USA).

All the experiments were performed under dry N_2 gas (20 ml min^{-1}). The samples were subjected to the following cycle: a heating ramp from − 50 to 200 °C, a cooling ramp from 200 to − 50 °C, and a second heating ramp from − 50 to 200 °C. All the heating/cooling ramps were performed at a scanning rate of 10 °C/min. The glass transition temperature (Tg), crystallization temperature (Tc), cold crystallization temperature (Tcc), melting temperature (Tm) and melting enthalpy (ΔHm) were determined from the first heating scan. The crystallinity percentage X in all investigated systems was evaluated as [30]:

$$X = \frac{\Delta H}{\Delta H_m^0} \cdot 100 \tag{1}$$

where: $\Delta H = \Delta H_m - \Delta H_{cc}$ (ΔHm and ΔHcc being the specific melting and cold crystallization enthalpies, respectively) and ΔH_m^0 is the melting enthalpy of a 100% crystalline PLA (93.0 J/g [31]) and PHB (146.0 J/g [32]).

X-ray Powder Diffraction (XRD)

X-ray diffraction-analyses (XRD) were performed on compression molded specimens, using PANalytical X'PERT PRO with Cu–KX-ray source (1.540562 Å) and a scanning rate of $0.026°\text{min}^{-1}$.

Rheological Measurements

Rheological measurements were performed using an ARES TA Instrument (New Castle, USA) rheometer with parallel plate geometry (plate diameter = 25 mm), under nitrogen atmosphere to avoid polymer oxidative degradation. Complex viscosity, elastic and loss moduli were measured performing frequency scans from 0.1 to 100 rad/s at 190 °C. The strain was fixed at $\gamma = 20\%$, which is low enough to be in the polymer linear viscoelastic regime. The typical gap between the plates imposed during the tests was 1 mm. Prior to the measurements, the samples were vacuum dried at 80 °C for 4 h.

Scanning Electron Microscopy (SEM)

The surface morphology of the blends was observed using a LEO-1450VP Scanning Electron Microscope SEM (beam voltage: 20 kV). The observations were performed on the cross-section of the samples, obtained through fracturing in liquid nitrogen. Before the tests, the fracture surface was coated with a thin gold layer.

Thermo-Mechanical Measurements (DMA)

DMA measurements were performed using Q800 TA Instrument (New Castle, USA) with tension film clamp. Samples 6 mm width × 26 mm height × 1 mm thickness were used. The temperature was varied in the range from 30 to 120 °C, applying a heating rate of 3 °C/min. The test conditions were: 1 Hz of frequency in strain-controlled mode with 15 m of amplitude, static loading of 125% of dynamic loading and 0.01 N of preload. Samples were vacuum dried at 80 °C for 4 h before the tests. The thermo-mechanical tests were carried out on 3 tests for each sample with an error less than 1%.

Results and Discussion

Thermodynamics of Clay Localization

The thermodynamics localization of the filler can be predicted through determining the wetting coefficient ω_a, in a thermodynamic equilibrium state. It depends on the interfacial energies γ_{xy} where x or y is polymer A, polymer B or clay according to the Young's equation [33], which is defined as:

$$\omega_a = \frac{\gamma_{clay-polymer\,B} - \gamma_{clay-polymer\,A}}{\gamma_{polymer\,A-polymer\,B}} \tag{2}$$

If $\omega_a > 1$ the clay will be preferentially dispersed in polymer A, if $\omega_a < -1$ the clay be located in polymer B and for $-1 < \omega_a < 1$ the clay will be located at interfaces between polymers A and B. Since the determination of the interfacial energies between clay and polymers is difficult, these were estimated using surface energies, which consist of dispersive γ^d and polar γ^p components [34]:

$$\gamma_x = \gamma_x^d + \gamma_x^p \tag{3}$$

$$\gamma_y = \gamma_y^d + \gamma_y^p \tag{4}$$

These two components of surface energy can be used to calculate interface energy using the harmonic-mean equation [35]:

$$\gamma_{xy} = \gamma_x + \gamma_y - 4\left(\frac{\gamma_x^d \gamma_y^d}{\gamma_x^d + \gamma_y^d} + \frac{\gamma_x^p \gamma_y^p}{\gamma_x^p + \gamma_y^p}\right) \tag{5}$$

and the geometric-mean equation [36]:

$$\gamma_{xy} = \gamma_x + \gamma_y - 2\left(\sqrt{\gamma_x^d \gamma_y^d} + \sqrt{\gamma_x^p \gamma_y^p}\right) \tag{6}$$

The surface tension levels reported in the literature have been measured at room temperature and need to be corrected for the processing temperature, i.e. 190 °C. To this aim, the Guggenheim equation developed for small molecule liquids can be applied to polymers to calculate surface tension levels at the desired temperatures [37]:

$$-\frac{\partial \gamma}{\partial T} = \frac{11}{9} \frac{\gamma_0}{T_c}\left(1 - \frac{T}{T_c}\right) \tag{7}$$

where γ_0 is the surface tension at T = 0 and Tc represents the critical temperature. The value of $-d\gamma/dT$ relative to the polymers and the filler was taken from the literature [37]. The total surface energy γ ($\frac{Nm}{m}$) at room temperature (25 °C) and at processing temperature (190 °C), the dispersive γ^d

Table 2 Surface energy at room temperature and processing temperature for each component

	Room temperature		Process temperature		
	$\gamma \left(\frac{Nm}{m} \right)$	$-\frac{\partial \gamma}{\partial T} \left(\frac{Nm}{m \,°C} \right)$	$\gamma^d \left(\frac{Nm}{m} \right)$	$\gamma^p \left(\frac{Nm}{m} \right)$	$\gamma \left(\frac{Nm}{m} \right)$
PLA	40.6 [38]	0.06 [38]	27.4	3.4	30.8
PHB	46.9 [39]	0.06 [39]	28.18	8.82	37
Cloisite 5	42.54 [40]	0.1 [41]	16.9	6	22.9

Table 3 Interfacial energies calculated from harmonic-mean equation and geometric-mean equation

	Harmonic-mean	Geometric-mean
$\gamma_{clay\text{-}PHB}$	3.35	1.70
$\gamma_{clay\text{-}PLA}$	3.10	1.57
$\gamma_{PLA\text{-}PHB}$	2.35	1.23

$(\frac{Nm}{m})$ and the polar γ^p $(\frac{Nm}{m})$ components at 190 °C of PLA, PHB and Cloisite 5 have been summarized in Table 2.

Based on the values of surface tensions, the interfacial tension between pairs of components clay-polymer B, clay-polymer A and polymer A-polymer B, where polymer A is PLA and polymer B is PHB, was calculated according to Eqs. (5) and (6) and the data are shown in Table 3.

The values of the wetting coefficient, calculated though Eq. (2), are 0.11 and 0.10 using the energy surface calculated with the harmonic-mean equation and geometric-mean equation, respectively. The obtained values suggest that the organoclays are located at the interface between PLA and PHB, based on thermodynamic preference.

Influence of Screw Profiles and Screw Speed

Figure 2a displays the DSC curves recorded during the first heating runs for neat PLA, PHB and PLA/PHB blend. Neat PLA exhibits a glass transition temperature at 60 °C [42], a melting temperature at 170 °C and a cold crystallization peak at 100 °C [43]. Neat PHB shows a glass transition temperature at about 3 °C and double fusion peak at 108 °C and 132 °C. Concerning to PLA/PHB, the blend shows a glass transition temperature at 60 °C attributed to the PLA phase [44]. Furthermore, an exothermic peak at 95 °C and an endothermic one at 170 °C can be observed. These peaks, in agreement with the aforementioned results, can be associated to the cold crystallization and the melting of PLA phase, respectively.

Figure 2b reports the thermograms recorded for the unfilled blend, previously discussed, and the filled blends processed by different screw profiles. In the filled blends the values of the glass transition temperatures of PLA and PHB, the cold crystallization temperature of PLA and the melting peaks relative to the PLA and PHB are unchanged compared to the unfilled sample.

Table 4 reports the main thermal properties, namely cold crystallization enthalpy (ΔHcc), melting enthalpy (ΔHm) and crystallinity degree (X) measured during the first heating ramp for all the formulations. The crystallinity degree of PLA increases from 11 to 18% when PHB is introduced in the blend, due to the ability of PHB to act as nucleating agent, enhancing the recrystallization of PLA [45]. Regardless the selected screw profile and screw speed, the introduction of the clay nanoparticles induces a decrease of the crystallinity degree of PHB phase. On the contrary, a different behavior can be observed regarding the influence of the embedded nanoclays on the crystallinity of PLA; in fact, the nanoparticles cause an increase of the crystalline
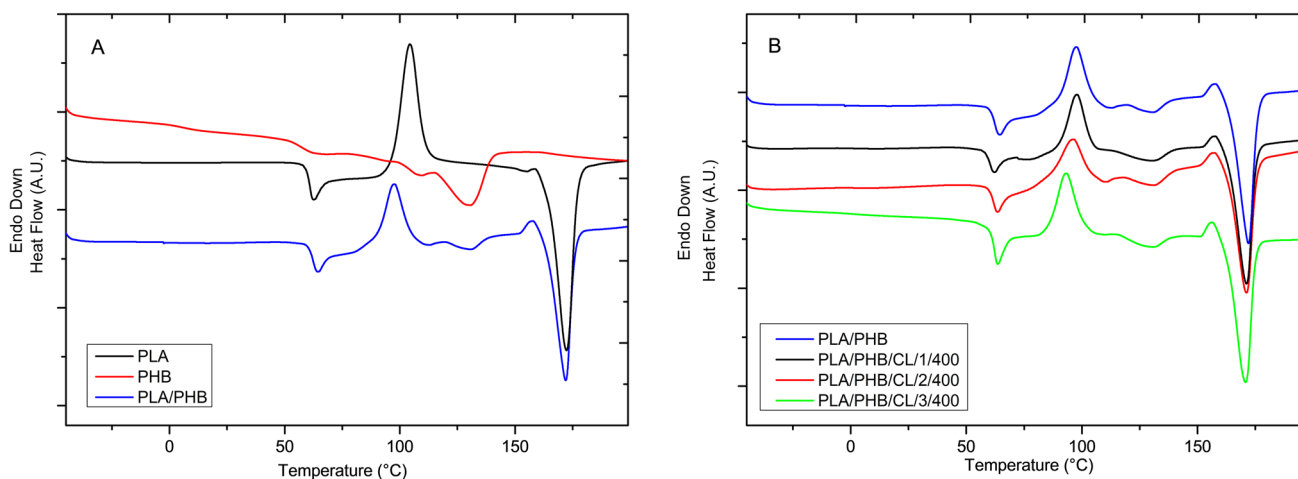
Fig. 2 DSC thermograms recorded during the first heating scans for **a** neat PLA and PHB and PLA/PHB blend **b** filled blends with different screw profiles

Table 4 Thermal properties of PLA, unfilled blend and filled systems with different screw profiles and screw speed

	$\Delta H_{m(PLA)}$ [J/g]	$\Delta H_{cc(PLA)}$ [J/g]	$X_{(PLA)}$ [%]	$\Delta H_{m(PHB)}$ [J/g]	$X_{(PHB)}$ [%]
PLA	46	36	11	–	–
PHB	–	–	–	17	12
PLA/PHB	38	21	18	4	3
PLA/PHB/CL/1/400	36	17	22	5	4
PLA/PHB/CL/2/400	36	18	20	5	4
PLA/PHB/CL/3/400	39	19	23	6	4
PLA/PHB/CL/3/250	29	14	17	5	4
PLA/PHB/CL/3/550	40	19	24	5	4

content due to their well-known nucleating effect, facilitating the crystallization process [46]. However, this effect is more pronounced for blends processed with screw profiles 1 and 3 and specially at high screw speed.

Figure 3 shows the diffractograms obtained from XRD analysis relative to the neat polymers PLA and PHB and unfilled blend (Fig. 3a) and unfilled and filled blends, along with that of the nanoclays (Fig. 3b). As to concern the neat PHB, the diffractogram exhibits two peaks at $2\theta = 13.9°$ and $16.8°$ associable with the (020) and (110) of orthorhombic unit cell respectively [47, 48]. Otherwise, PLA shows an amorphous structure [49]. The pattern of the unfilled polymer blend is similar to that of neat PHB and a peak at about $19°$ attributable to the PLA phase, appears. This peak is usually present in fully crystallized PLA samples, indicating that the addition of PHB crystal particles significantly improves the crystallinity and the crystallization rate of PLA, according with DSC results which suggested an increase of the degree of crystallinity of PLA in the blend [50].

Figure 3b reports the diffractogram of filled blend processed with different screw profiles. Interestingly, the ratio between the intensities of the peaks related to PHB is different with respect of neat polymer, indicating a modification of the PHB crystal structure resulting from the interactions between PHB and PLA [50]. In fact, the crystallinity of PHB in unfilled and filled blends is lower than in the neat polymer, as already inferred from DSC results.

The clay particles exhibit a distinct peak at about $2\theta = 7°$, corresponding to a distance between layers calculated by Bragg's law [51] of $d_{001} = 1.26$ nm, and two further peaks at $2\theta = 19.7°$ and $22°$. In spite of that, to investigate the interaction of the clay with polymers, it is fundamental the analysis of the first peak. In filled blends obtained with screw profile 1 and 3 the interlayer distance corresponds to $d_{001} = 1.77$ nm and this value remains unchanged by varying the speed of the screw. Differently, in filled blend processed with screw profile 2 a value of $d_{001} = 1.47$ nm was obtained. The observed increase of the interlayer distance can be associated with the insertion of polymer chains between the clay platelets, leading to the formation of an intercalated structure
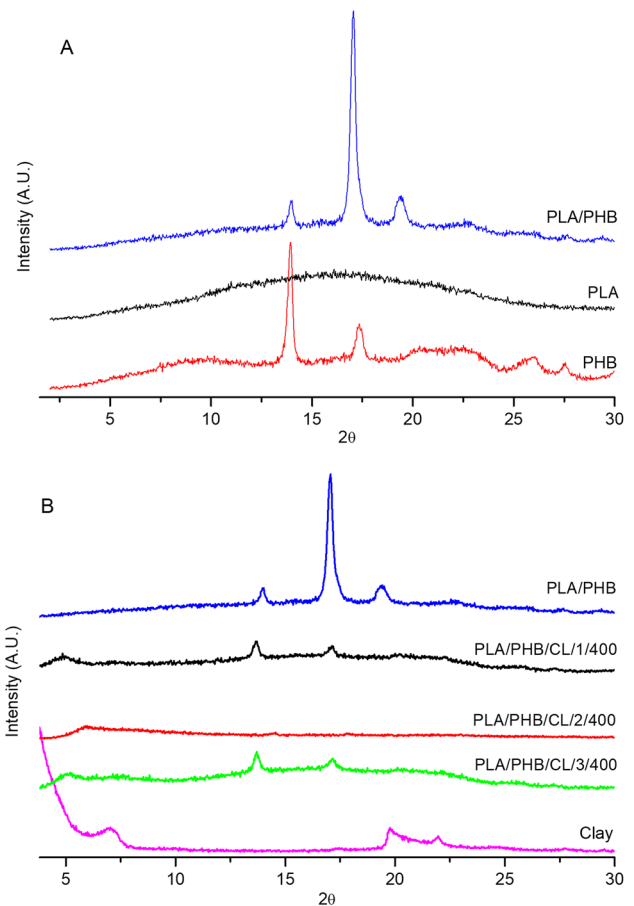
Fig. 3 XRD pattern of **a** neat PLA, neat PHB and unfiled blend, **b** clay, PLA/PHB blend and PLA/PHB/CL processed with different screw profiles

[52]. The obtained results suggest that screw profiles 1 and 3 allow a good dispersion of the filler by promoting a better intercalation of the polymers in the nanoclay structure.

Rheological analyses in linear dynamic shear flow have been carried out in order to evaluate the effect of the nanoclays on the microstructure of the blends. In fact, the evaluation of the rheological behaviour of polymer-filled based blends represents an effective tool to investigate the

established polymer/filler and polymer/polymer interactions, allowing to obtain important information about the morphology of the blend. Figure 4 shows the rheological results for the filled blends processed with all selected screw profiles and a representative curve of unfilled blend.

For all filled blends, an increase of the G′ modulus can be observed, as compared to the values of the unfilled blend, and this finding is more pronounced in the low frequency region. In particular, as clearly observable in Fig. 4a, PLA/PHB exhibits the typical rheological response of an immiscible blend, with the appearance of a shoulder at low-intermediate frequencies, which can be related to the relaxation of the dispersed phase that is in the form of droplets [53]. Filled blends, regardless of the adopted screw configurations, exhibit a remarkable different trend of G′ as a function of the frequency as compared to the unfilled blend, and the disappearance of the aforementioned shoulder can be noticed. This different behaviour can be attributed to the occurrence of strong polymer–filler interactions, promoting an improved blend morphology with respect to the unfilled systems [54]. Looking at the differences between the filled blends processed with the different screw configurations, in the case of the screw profile 1 the rheological response, at low frequencies, is different, and a lowering of the slope in the terminal region is observed. This behavior is also present in the filled blend obtained with screw profile 3, where the presence of backflow elements induced high shear stresses during the processing, causing a modification of the blend morphology. This phenomenon does not occur with screw profile 2, probably due to the absence of dispersion elements that do not promote optimal miscibility.

To further investigate the peculiar behaviour of the low-frequency trend of G' for filled blends obtained with different screw profiles, the slope of the curve was calculated according to Eq. (8)

$$\alpha(\omega) = \frac{d \log G'}{d \log \omega} \tag{8}$$

and the obtained curves are reported in Fig. 4b.

The curve of the unfilled blend shows a progressive decrease of the G′ slope with increasing the frequency, reflecting the relaxation of a single dynamic specie related to the droplets constituting the dispersed phase. Differently, the curves of the filled blends, remain almost constant over the whole tested frequency range, indicating the presence of particles of dispersed phase of different shapes and dimensions, which are able to relax at different time scales [21].

Figure 5 shows the trend of G′ of the formulation obtained using screw profile 3, processed at different screw speeds. At low frequencies the filled blend processed at 250 rpm shows a lower G′ value than those obtained at 400 and 550 rpm; therefore, an increase of screw speed improved the interaction filler-polymers, and consequently an increase of G′ value [55], notwithstanding the invariance of the trend of the curve in the three cases.
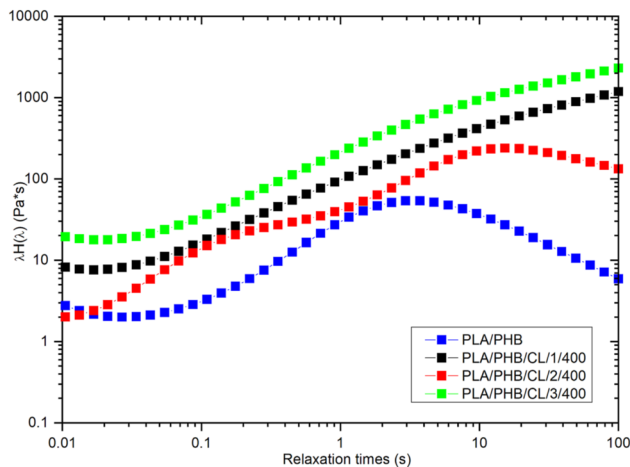
The weighted relaxation spectra of the filled and unfilled blends processed with different screw profiles are plotted in Fig. 6. This representation allows to distinguish any changes in the microstructure of a multi-component polymer-based system through the discrimination of the different relaxation process [56]. The weighted relaxation spectrum (λH(λ)) can be calculated with data coming from small amplitude oscillatory shear measurements, using the method proposed by Honerkamp and Weese [57], which
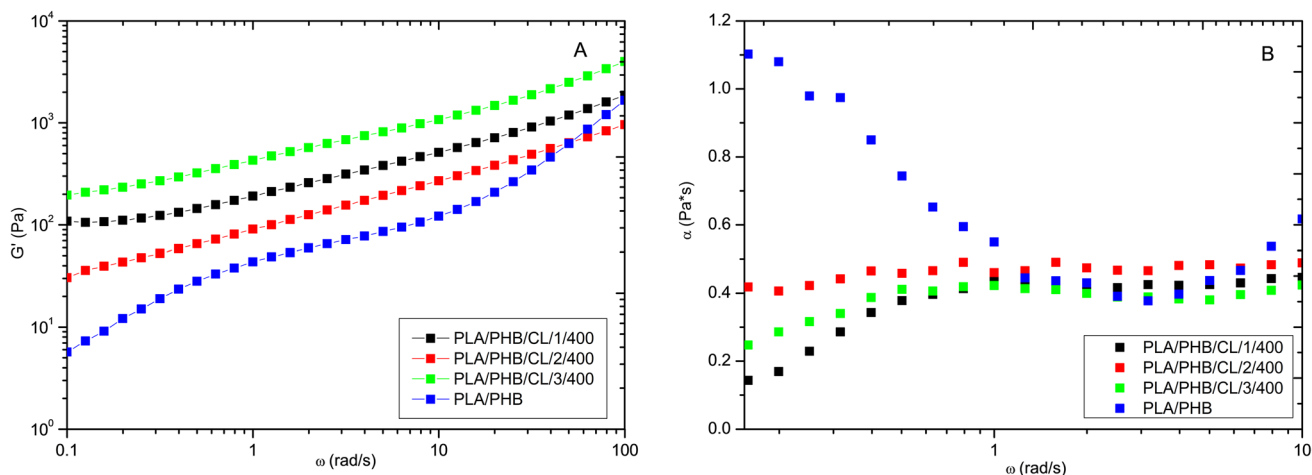
Fig. 4 Evolution of **a** storage modulus of filled blends with different screw profiles and **b** α as a function of frequency in filled blends obtained with different screw profiles
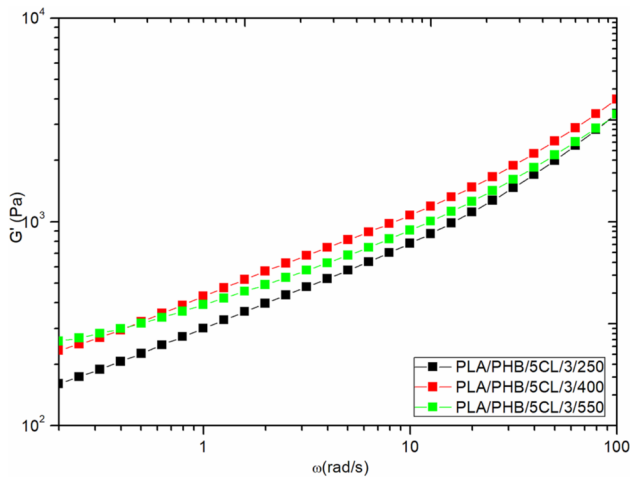
Fig. 5 Evolution of storage modulus of filled blend screw profile 3 at different screw speed

Fig. 6 Weighted relaxation spectra for unfilled and filled blends processed with different screw profiles

is based on the response of an infinite number of Maxwell models placed on parallel:

$$G'(\omega) = \int_{-\infty}^{+\infty} H(\lambda) \frac{\omega^2\lambda^2}{1+\omega^2\lambda^2} d\ln\lambda \qquad (9)$$

$$G'(\omega) = \int_{-\infty}^{+\infty} H(\lambda) \frac{\omega\lambda}{1+\omega^2\lambda^2} d\ln\lambda \qquad (10)$$

where G′(ω) and G″(ω) are storage modulus and loss modulus measured through the frequency sweep tests, H(λ) the relaxation time spectrum and λ the relaxation time, respectively.

In the case of a polymer-based blend, the peaks at short relaxation times are associated to the relaxation of the blend constituents, while the signals observed at longer times are attributed to the relaxation processed of the interfaces. PLA/PHB blend shows a peak between 1 and 10 s (at about 3 s) attributable to the shape-relaxation of the PHB dispersed droplets [58]. Furthermore, a rapid decrease of the H(λ) function is observed at longer times, indicating the fully relaxation of the PHB droplets in the considered time interval. It is important to highlight that the peak associated with the relaxation of PLA macromolecules is not present due to the very fast relaxation time $(10^{-3} < t < 10^{-2}$ [58]) of this polymer.

As far as the PLA/PHB/CL system processed with screw profile 2 is concerned, the relaxation spectrum is very similar to that of the unfilled blend, notwithstanding the shift of the peak related to the shape relaxation of PHB particles towards longer times, due to the slowing down of the relaxation dynamics of the droplets of the dispersed phase, induced by the presence of the embedded clay particles. This finding suggests that the screw profile 2 is not able to induce remarkable alteration of the material morphology, which remained almost unchanged with respect to that of the unfilled blend. A very different behaviour can be observed for the filled blends obtained with screw profiles 1 and 3. In fact, the peak associated with the relaxation process of the droplets of the dispersed phase is broader as compared to that of the unfilled blend, indicating the presence of various dynamic species relaxing at different times, associable with several populations of PHB particles characterized by different shapes and sizes. Besides, this peak is shifted towards longer times with respect to the unfilled blend, with the formation of a distinct tail at high relaxation times; this finding suggests that the relaxation mechanism of the particles of the dispersed phase is not fully completed in the investigated time range. The obtained results can be explained considering the coupled effect of the selected screw profiles and of the presence of well-dispersed clay nanoparticles. More specifically, the presence of distribution and backflow elements in the screw profiles 1 and 3 induced a significant modification of the blend morphology during the processing, allowing at the same time a more homogeneous dispersion of the embedded clay nanoparticles which in turn, being preferentially located at the interface between the two polymers, induced a further refinement of the material morphology.

The morphology of all formulations was evaluated through SEM observations. Representative micrograph of PLA/PHB blend, reported in Fig. 7a, shows roughly spherical PHB particles (having dimension of about 3 μm) dispersed in the PLA matrix. This morphology confirms the immiscibility between polymers at this explored weight ratio predicted in all the characterizations above discussed.
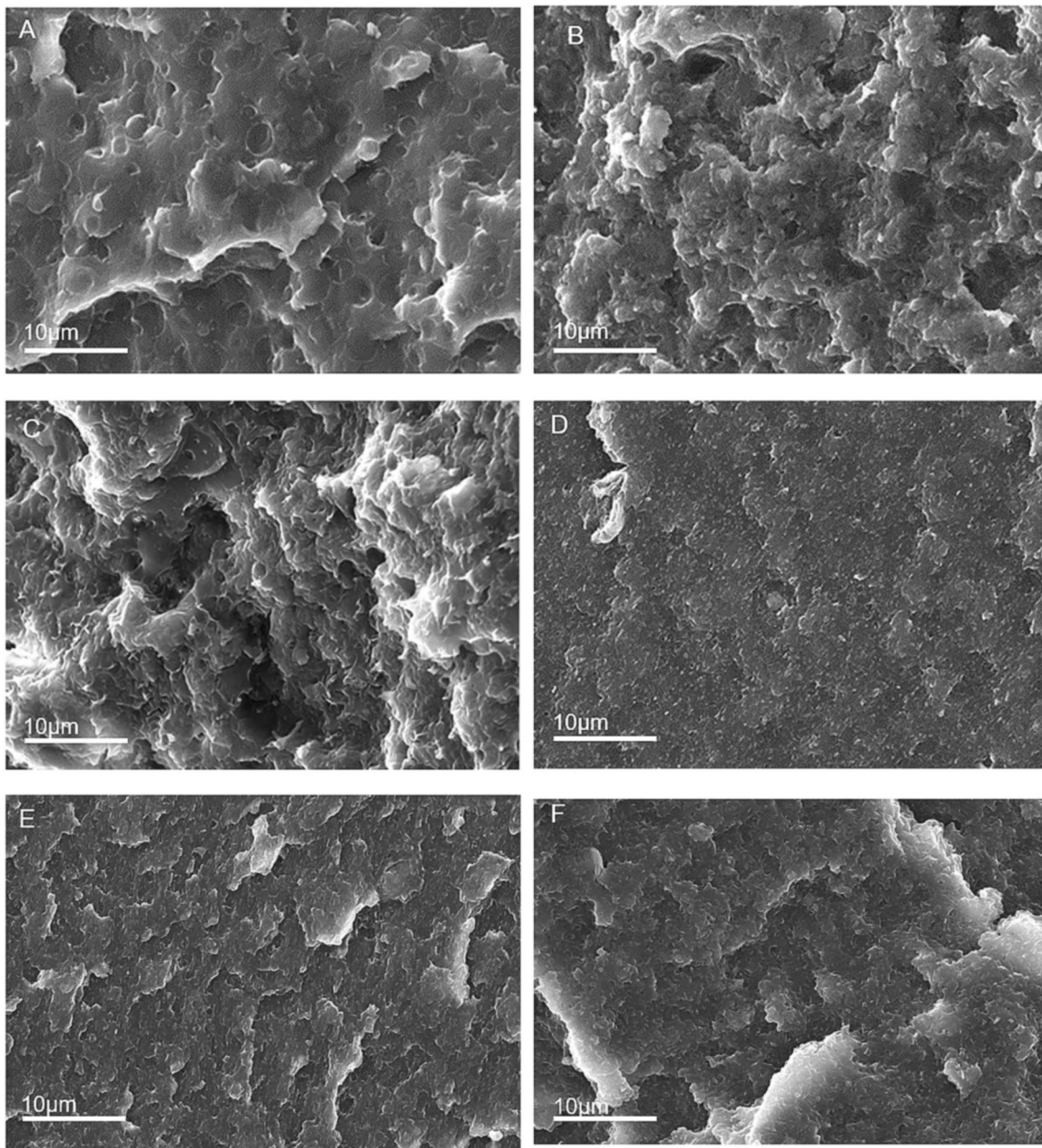
Fig. 7 SEM micrographs of fractured surface of **a** PLA/PHB, **b** PLA/PHB/CL/1/400, **c** PLA/PHB/CL/2/400, **d** PLA/PHB/CL/3/400, **e** PLA/PHB/CL/3/250 and **f** PLA/PHB/CL/3/550

Figure 7b–d show the micrographs of the filled blends obtained through the different screw profiles. In particular, the filled blend obtained with screw profile 2 (Fig. 7c) shows a droplets configuration: during the fracturing most of the PHB particles remained in the structure, while others were pulled out, leaving empty cavities on the surface. Despite this, a weak improvement of the morphological structure of this filled blend compared to the unfilled one can be noticed.

Conversely, in the filled blends processed by screw profile 1 and 3, a clear modification of the microstructure is observable. In particular, no droplet structures are observable at the

investigated magnification level. The refinement of the morphology noticed in these formulations is caused by the specific design of the screw profiles that allows a good polymers/clay interaction level with the consequent formation of intercalated structures of polymer chains into the clay, as already discussed in XRD results. However, this result is a consequence of the coupled effect of the nanoclay presence and the selected screw configuration: the flow conditions established during processing due to the presence of dispersion elements (screw profile 1) and backflow (screw profile 3), cause the achievement of a
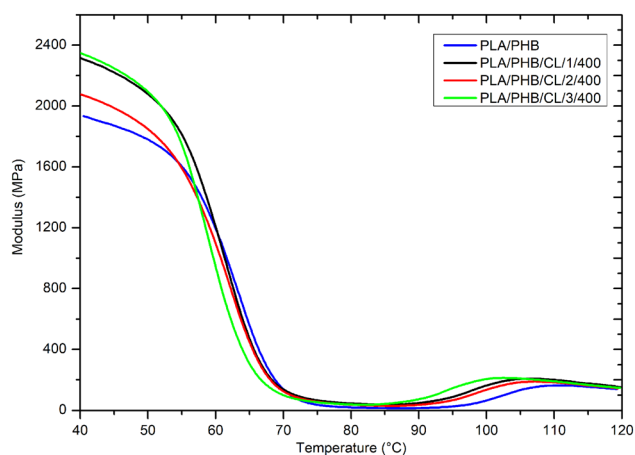
Fig. 8 DMA traces for PLA/PHB and PLA/PHB/CL blends processed with different screw profiles

Table 5 Thermo-mechanical properties of PLA/PHB and PLA/PHB/CL blends

	$T_{tan\ delta}$ [°C]	Modulus [MPa] @ 40 °C
PLA/PHB	72	1996
PLA/PHB/CL/1/400	73	2310
PLA/PHB/CL/2/400	73	2064
PLA/PHB/CL/3/250	71	2245
PLA/PHB/CL/3/400	72	2326
PLA/PHB/CL/3/550	72	2294

good interaction between filler and polymers [59], promoting the obtainment of a refined morphology.

The screw speed variation (Fig. 7e and f) has a lower impact on the modification of the material morphology, as compared to the variation of screw profile. In fact, the samples show a similar morphology, according to rheological results where no remarkable alterations of the relaxation behaviour of filled blends was detected.

Furthermore, dynamic thermomechanical analyses were carried out and Fig. 8 reports the curves of storage modulus as a function of temperature for unfilled and filled blends. The rapid decrease of the storage modulus at about 60–70 °C is attributed to the glass transition of the PLA [60]. Besides, the increase of storage modulus observed at 90–110 °C is associable to the cold crystallization of PLA [61]. All the filled samples show, as expected, an increase of the modulus value, as compared to their unfilled counterparts, due to the reinforcing effect of the well-dispersed nanofillers [62]. In particular, in the cases of the filled blends obtained with screw profiles 1 and 3, the increase of the modulus at 40 °C is about of 20%, whereas in the screw profile 2, this improvement is only about 9%; this finding indicates that screw profiles 1 and 3 are more effective in inducing an enhancement of the thermo-mechanical properties of the filled blends as compared to screw profile 2.

Table 5 shows the values of tan delta and storage modulus at 40 °C of the filled blend processed with screw profile 3 at different rpm. Particularly, the modulus is slightly higher for the blends processed with higher screw speeds (400 rpm and 550 rpm).

Conclusions

In this work, the influence of process parameters on the microstructure and properties of PLA/PHB/clay blend nanocomposite was assessed. In particular the influence of the screw profile and screw speed were evaluated.

The clay nanofillers, preferentially localized at the interface between PLA and PHB, exert a nucleating action, inducing an increase of the crystallinity content of PLA (+ 25%), especially in filled blend processed with screw profile 1 and 3. Results coming from XRD analysis indicate that the design of screw 1 and 3 promotes a dispersion of the embedded nanofillers bringing about to the achievement of by intercalated structures. This finding reflects in the thermo-mechanical properties of filled blends as an improvement of modulus due to the reinforcing effect of the clay: the increase is about of 20% in filled blend processed through screw profile 1 and 3 and 9% in the material obtained by using screw profile 2.

Additionally, a detailed rheological characterization allowed assessing a remarkable effect of the selected screw profile on the polymer relaxation dynamics; more specifically, the relaxation behaviour of nanofilled blends processed through screw profiles 1 and 3 indicates an arrestment of the relaxation processes of polymer macromolecular chains, due to the establishment of intense polymer-filler interactions in the interfacial region. Differently, nanofilled blend processed with screw profile 2 shows a rheological response quite similar to that of the unfilled blend, suggesting that the selected screw design is less effective in inducing significant alterations of the blend microstructure.

SEM observations confirmed the above results, since the specific design of the screw (screw profile 1 and 3) allowed to achieve a more refined morphology as compared to the unfilled systems, due to the coupled effect of the high shear stresses that polymers experienced during processing and the presence of well-dispersed nanoclays, further helping in stabilizing the blend microstructure.

To sum up, the results revealed a remarkable effect of the screw profile and the presence of the filler on the

microstructure and thermal and thermo-mechanical properties of the blend. The final characteristics of the nanocomposites, on the other hand, were not significantly affected by the screw speed using the same profile. These results demonstrated the potential applications for these materials as rigid packaging, personal care and cosmetic products, toys [63] given that in recent years the development of biopolymers was addressed also toward the production of durable parts. In this context, filled bio-blends and their processing behavior play a key role in the possibility to obtain materials with tunable properties and characteristics.

Declarations

Conflict of interest The authors declare no conflict of interest.

References

1. Babu RP, O'Connor K, Seeram R (2013) Progr Biomater 2:1–16
2. Reddy MM, Vivekanandhan S, Misra M, Bhatia SK, Mohanty AK (2013) Progr Polym Sci 38:1653–1689
3. He Y, Hu Z, Ren M, Ding C, Chen P, Gu Q, Wu Q (2014) J Mater Sci Mater Med 25:561–571
4. Somleva MN, Snell KD, Beaulieu JJ, Peoples OP, Garrison BR, Patterson NA (2008) Plant Biotechnol J 6:663–678
5. Możejko-Ciesielska J, Kiewisz R (2016) Microbiol Res 192:271–282
6. Coffin DR, Fishman ML (1994) J Appl Polym Sci 54:1311–1320
7. Morro A, Catalina F, Corrales T, Pablos JL, Marin I, Abrusci C (2016) Carbohydr Polym 149:68–76
8. Bayer EA, Lamed R, Himmel ME (2007) Curr Opin Biotechnol 18:237–245
9. Burzic I, Pretschuh C, Kaineder D, Eder G, Smilek J, Másilko J, Kateryna W (2019) Eur Polym J 114:32–38
10. Requena R, Jiménez A, Vargas M, Chiralt A (2016) Polym Test 56:45–53
11. Muller J, González-Martínez C, Chiralt A (2017) Materials 10:952
12. Jin FL, Hu RR, Park SJ (2019) Compos B Eng 164:287–296
13. Li X, Yan X, Yang J, Pan H, Gao G, Zhang H, Dong L (2018) Polym Eng Sci 58:1868–1878
14. Dell'Erba R, Groeninckx G, Maglio G, Malinconico M, Migliozzi A (2001) Polymer 42:7831–7840
15. Ma P, Hristova-Bogaerds DG, Lemstra PJ, Zhang Y, Wang S (2012) Macromol Mat Eng 297:402–410
16. Graziano A, Jaffer S, Sain M (2019) J Elastomers Plast 51:291–336
17. Chen G, Shi T, Zhang X, Cheng F, Wu X, Leng G, Huang Z (2020) Polymer 186:122012
18. Arrieta MP, Samper MD, Aldas M, López J (2017) Materials 10:1008
19. Dawin TP, Ahmadi Z, Taromi FA (2019) Prog Org Coat 132:41–49
20. Lai SM, Liu YH, Huang CT, Don TM (2017) J Polym Res 24:1–12
21. D'Anna A, Arrigo R, Frache A (2019) Polymers 11:1416
22. Mochane MJ, Sefadi JS, Motsoeneng TS, Mokoena TE, Mofokeng TG, Mokhena TC (2020) Polym Compos 41(7):2968–2979
23. Müller K, Bugnicourt E, Latorre M, Jorda M, Echegoyen Sanz Y, Lagaron JM, Pérez G (2017) Nanomaterials 7(4):74
24. Da Silva GP, De Lima CJB, Contiero J (2015) Catal Today 257:259–266
25. Sivanjineyulu V, Behera K, Chang YH, Chiu FC (2018) Compos Part A Appl Sci Manuf 114:30–39
26. Zembouai I, Kaci M, Zaidi L, Bruzaud S (2018) Polym Degrad Stab 153:47–52
27. Emin MA, Schuchmann HP (2017) Trends Food Sci Technol 60:88–95
28. Decol M, Pachekoski WM, Segundo EH, Pinheiro LA, Becker D (2020) J Appl Polym Sci 137(20):48711
29. Hejazi I, Sharif F, Garmabi H (2011) Mater Des 32(7):3803–3809
30. Gigante V, Aliotta L, Coltelli MB, Cinelli P, Botta L, La Mantia FP, Lazzeri A (2020) J Polym Sci 58(23):3264–3282
31. Turner J, Riga A, O'Connor A, Zhang J, Collins J (2004) J Therm Anal Calorim 75:257–268
32. Barham PJ, Keller A, Othun EL, Holmes PA (1984) J Mater Sci 19(9):2781–2794
33. Young T (1805) Philos Trans R Soc Lond 95:65–87
34. Fowkes FM (1964) Ind Eng Chem 56:40–52
35. Wu S (1973) J Adhes 5:39–55
36. Owens DK, Wendt RC (1969) J Appl Polym Sci 13:1741–1747
37. Dharaiya D, Jana SC (2005) Polymer 46:10139–10147
38. Mirzadeh A, Ghasemi H, Mahrous F, Kamal MR (2015) J Appl Polym Sci 132:48
39. Zubairi SI, Bismarck A, Mantalaris A (2015) J Teknol 75:1
40. Gomari S, Ghasemi I, Karrabi M, Azizi H (2012) J Polym Res 19(1):9769
41. Lewin M, Mey Marom A, Frank R (2005) Polym Adv Technol 16:429–441
42. Tri PN, Domenek S, Guinault A, Sollogoub C (2013) J Appl Polym Sci 129(6):3355–3365
43. Zhang L, Xiong C, Deng X (1996) Polymer 37(2):235–241
44. Arrieta MP, Fortunati E, Dominici F, Rayón E, López J, Kenny JM (2014) Carbohydr Polym 107:16–24
45. Arrieta MP, López J, Hernández A, Rayón E (2014) Eur Polym J 50:255–270
46. Das K, Ray D, Banerjee I, Bandyopadhyay NR, Sengupta S, Mohanty AK (2010) Misra M 118(1):143–151
47. Silverajah VS, Ibrahim NA, Zainuddin N, Yunus WMZW, Hassan HA (2012) Molecules 17(10):11729–11747
48. Hurrell BL, Cameron RE (1998) J Mat Sci 33:1709–1713
49. Sun X, Guo L, Sato H, Ozaki Y, Yan S, Takahashi I (2011) Polymer 52:3865–3870

50. Zhang M, Thomas NL (2011) Adv Polym Technol 30(2):67–79
51. Elton LRB, Jackson DF (1966) Am J Phys 34(11):1036–1038
52. Abbasi F, Tavakoli A, Razavi Aghjeh MK (2018) J Vinyl Addit Technol 24(1):18–26
53. Castro M, Carrot C, Prochazka F (2004) Polymer 45:4095–4104
54. Remili C, Kaci M, Benhamida A, Bruzaud S, Grohens Y (2011) Polym Degrad Stabil 96:1489–1496
55. Dil EJ, Favis BD (2015) Polymer 76:295–306
56. Arrigo R, Mascia L, Clarke J, Malucelli G (2021) Polymers 13(2):276
57. Honerkamp J, Weese J (1993) Rheol Acta 32(1):65–73
58. Lacroix C, Aressy M, Carreau PJ (1997) Rheol Acta 36:416–428
59. Potente H, Bastian M (2001) Int Polym Process 16(1):14–30
60. Bai Z, Dou Q (2018) J Polym Environ 26(3):959–969
61. Cristea M, Ionita D, Iftime MM (2020) Mater 13(22):530
62. Dean K, Yu L, Bateman S, Wu DY (2007) J Appl Polym Sci 103(2):802–811
63. European Bioplastics. https://www.european-bioplastics.org/market/applications-sectors/

Publisher's Note Springer Nature remains neutral with regard to jurisdictional claims in published maps and institutional affiliations.